energies

MDPI

Article

# Enhanced Thermoelectric Properties of $Cu_3SbSe_3$-Based Composites with Inclusion Phases

**Rui Liu, Guangkun Ren, Xing Tan, Yuanhua Lin * and Cewen Nan**

State Key Laboratory of New Ceramics and Fine Processing, Tsinghua University, Beijing 100084, China; liur15@mails.tsinghua.edu.cn (R.L.); rgk13@mails.tsinghua.edu.cn (G.R.); tanx14@mails.tsinghua.edu.cn (X.T.); cwnan@mail.tsinghua.edu.cn (C.N.)

* Correspondence: linyh@mail.tsinghua.edu.cn; Tel.: +86-10-6277-3741

Academic Editor: Zhi-Gang Chen

Received: 18 August 2016; Accepted: 9 October 2016; Published: 14 October 2016

**Abstract:** $Cu_3SbSe_3$-based composites have been prepared by self-propagating high-temperature synthesis (SHS) combined with spark plasma sintering (SPS) technology. Phase composition and microstructure analysis indicate that the obtained samples are mainly composed of $Cu_3SbSe_3$ phase and $CuSbSe_2$/$Cu_{2-x}Se$ secondary phases. Our results show that the existence of $Cu_{2-x}Se$ phase can clearly enhance the electrical conductivity of the composites (~16 S/cm), which is 2.5 times higher than the pure phase. The thermal conductivity can remain at about 0.30 $W \cdot m^{-1} \cdot K^{-1}$ at 653 K. A maximum $ZT$ (defined as $ZT = S^2\sigma T/\kappa$, where $S$, $\sigma$, $T$, $\kappa$ are the Seebeck coefficient, electrical conductivity, absolute temperature and total thermal conductivity) of the sample SPS 633 can be 0.42 at 653 K, which is 60% higher than the previously reported values. Our results indicate that the composite structure is an effective method to enhance the performance of $Cu_3SbSe_3$.

**Keywords:** $Cu_3SbSe_3$; $Cu_{2-x}Se$; electrical conductivity; spark plasma sintering (SPS)

## 1. Introduction

The worldwide demand for energy is causing restless agitation. The combustion of fossil fuels generates a large amount of unused waste heat that can be converted to electricity by thermoelectrics [1,2]. The efficiency of thermoelectric (TE) material is mainly decided by the materials' dimensionless figure of merit $ZT$ [3]. A lager $ZT$ helps to achieve a relatively higher efficiency. To improve the $ZT$ value, reducing thermal conductivity has been proved to be effective [4]. Therefore, many kinds of TE materials with low thermal conductivity such as layered oxide BiCuSeO [5], $Cu_{2-x}Se$ [6] and SnSe [7,8] have been widely studied.

Recently, Cu-Sb-Se ternary compounds with a diamond like tetrahedral structure have come into consideration because of low thermal conductivity. However, their poor electric properties lead to relatively low $ZT$. In fact, $Cu_3SbSe_4$ which is a p-type semiconductor with a small band gap attracts much more attention [9]. $Cu_{12}Sb_4Se_{13}$ is predicted to be a new promising TE material theoretically [10], the structure of which is similar to tetrahedrites $Cu_{12}Sb_4S_{13}$ [11], but this compound has not been synthesized yet. $Cu_3SbSe_3$ and $CuSbSe_2$ both have ultralow thermal conductivity that was thought to be governed by a large lattice anharmonicity [12] caused by lone-pair electron of Sb [13]. Compared with widely studied $Cu_3SbSe_4$, researches of $Cu_3SbSe_3$ are inadequate because it is difficult to obtain the single phase [14] and they have poor TE properties [15]. After being sealed in quartz ampoules and followed by a long-time annealing, there are still other phases [16]. Up to now, $Cu_3SbSe_3$ has been fabricated by vacuum melting [13] or mechanical alloying [17], and such long-time synthesis as well as high energy consumption are obstacles to the commercial applications of some content. A relatively low $ZT$ of 0.25 at 650 K was achieved by others [17]. By contrast, SHS has been proved as

an efficient method to synthesize thermoelectric materials [18], which could significantly save time and energy simultaneously. Numerous materials have been obtained by this method [18–22].

In this work, we make use of the easy transition in a Cu-Sb-Se ternary system to generate other phases in situ instead of wasting time and energy to obtain the single phase, which shows bad thermoelectric performance. $Cu_3SbSe_3$-based TE material consisting of $Cu_3SbSe_3$, $CuSbSe_2$, and $Cu_{2-x}Se$ has been prepared by SHS in a short duration for the first time. As a result, significant enhancement in the electrical conductivity and thermoelectric power factor ($S^2\sigma$) were achieved while keeping the ultralow thermal conductivity. Meanwhile, we find the appropriate temperature of spark plasma sintering (SPS). The maximum $ZT$ of 0.42 at 653 K is obtained in the sample SPS 633 which is the highest of $Cu_3SbSe_3$-based TE material so far.

## 2. Experimental Section

In the initial stage, Cu (99.9%, Aladdin, Shanghai, China), Sb (99.85%, Aladdin) and Se (99.99%, Aladdin) powders were mixed in stoichiometric amounts and then were cold-pressed into pellets of $\phi$ = 20 mm. The obtained pellets were brought to ignition point with a torch flame. After about 2 min, the combustion process appeared. And the process of combustion with different heating rates is shown in the differential scanning calorimeter (DSC) curve. The bulks were then grounded into fine powders. Then they were compacted into pellets of $\phi$ = 12.7 mm by SPS (Sumitomo Coal Mining Co. Ltd., Tokyo, Japan) at the temperature of 593, 613, 633, 653 and 673 K for 5 min under a uniaxial pressure of 50 MPa.

The phase structures were investigated by X-ray diffraction (XRD, RINT2000, Rigaku, Tokyo, Japan) analysis. The morphologies of cross-sectional bulks with different SPS temperature were observed by field-emission scanning electron microscopy (FESEM, LEO1530, Oxford Instruments, Oxford, UK). The sintered samples were cut into squares of 10 mm × 10 mm and bar-shaped specimens of 10 mm × 3 mm × 3 mm. The Seebeck coefficients and electrical resistivity were measured from room temperature to 653 K with the bar-shape specimen by ZEM-3 (ULVAC, Kanagawa, Japan). The thermal diffusivity ($D$) and $C_p$ were obtained by laser flash method (LFA-457, Netzsch, Selb, Germany). The total thermal conductivity was calculated by the equation $\kappa = DC_p\varrho$, where $\varrho$ is the density of the sample measured by the Archimedes method. The elemental uniformity and phase distribution were determined by electron probe micro-analyzer (EPMA JXA-8230, JEOL, Tokyo, Japan). The combustion temperature and required heating speed were determined by DSC/thermal gravimetric analysis (DSC/TGA 1, Mettler Toledo, Greifensee, Switzerland) with Ar flowing at the rate of 60 mL/min.

## 3. Results and Discussion

Figure 1A shows the XRD patterns of the samples after SPS with different temperature (593, 613, 633, 653 and 673 K). As shown in the XRD results, the secondary phases of $Cu_{2-x}Se$ and $CuSbSe_2$ are clearly found. This is similar to a previous report [16]. Here the SHS method requires only a few seconds instead of being sealed in quartz ampoules for tens of hours. Meanwhile, in order to determine related thermodynamic parameters of the combustion process, we compared the DSC curve with different heating rates in Figure 1B.

We selected 10, 30, 50, 70 K·min$^{-1}$ as heating rates for DSC. For all the process, three peaks exist, two of which are exothermic peaks (a,c). The first peak represents the solid state reaction possibly, while the endothermic peak (b) corresponds to the melting points ($T_m$) of Se ($T_m \sim$ 493.3 K). When the heating rate was increased to 50 K·min$^{-1}$ or larger, the endothermic peak (b) becomes smaller with a bigger and wider exothermic peak (c) because of the large amount of heat generated by SHS process. The figure indicates that the SHS occurred when the heating rate achieved values larger than 50 K·min$^{-1}$ and the temperature achieved the lowest melting point of the compound ($T_m$ of Se).

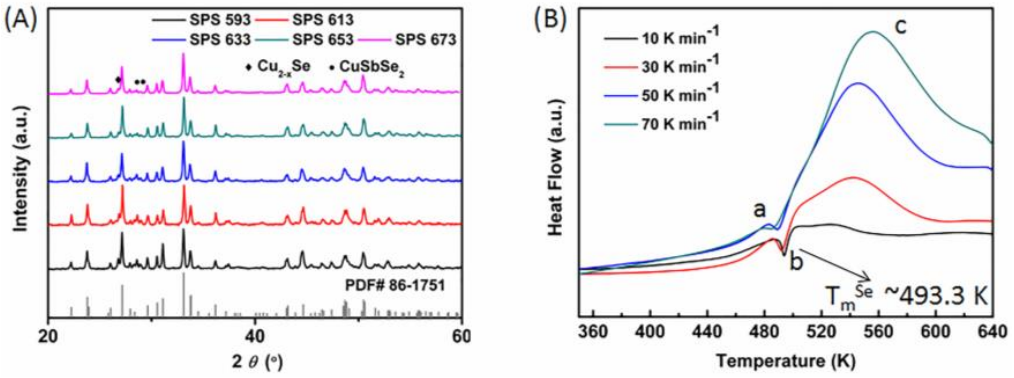


**Figure 1.** (**A**) X-ray diffraction (XRD) patterns of all the bulk samples; and (**B**) differential scanning calorimeter (DSC) of the powders with different heating rates.

The morphologies of cross-sectional bulks were characterized by SEM. As shown in Figure 2a–d, when the SPS temperature was lower than 633 K, the samples were not sintered well, and as a result, the white area or circle in Figure 2a,b appeared. As the SPS temperature was increased (shown in Figure 2c,d), the compaction of the samples without so many holes was improved, which can be seen in Figure 3. When elemental distribution was obtained by EPMA in Figure 2e, the sample phase was $Cu_3SbSe_3$ combined with $CuSbSe_2$ and $Cu_{2-x}Se$, which was in good agreement with XRD results. Elemental ratio Cu-Sb-Se of the black area in the Figure 2e is 62.5219:0.1380:37.3522, which represents $Cu_{2-x}Se$. The white part represents $CuSbSe_2$ (elemental ratio: 26.8254:24.5904:48.5842) while the grey area is $Cu_3SbSe_3$ (elemental ratio: 42.1054:14.3618:43.5328) as the main phase. The small deviation of elemental ratio might be caused by Se volatilization during the fabrication process.

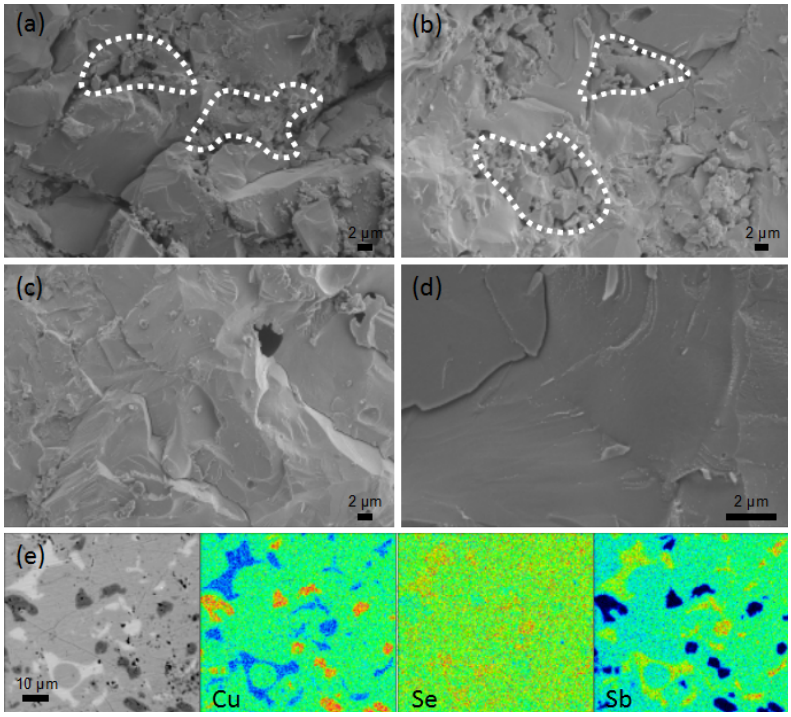


**Figure 2.** Scanning electron microscopy (SEM) images of (**a**) spark plasma sintering (SPS) 593; (**b**) SPS 613; (**c**) SPS 633 and (**d**) SPS 653 bulk samples; and (**e**) electron probe micro-analyzer (EPMA) images of SPS 633 bulk sample.

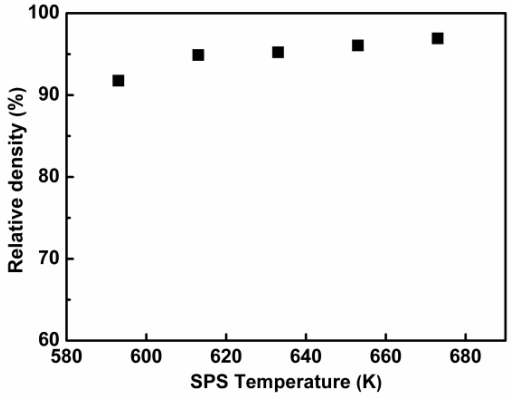


**Figure 3.** Relative density of all the bulk samples.

Figure 4 shows temperature dependence of the electrical conductivity and Seebeck coefficient. As the SPS temperature increases, the electrical conductivity increases until 633 K while σ is almost the same when the SPS temperature is higher than 633 K. The possible reason for this is the white circle mentioned above in Figure 2a,b. The electrical conductivity of all the samples increase with $T$, which indicates that the semiconductor properties did not change with the SPS temperature. Meanwhile, the SPS 633 sample finally reaches to 16 S/cm at 653 K which is nearly 2.5 times higher than previous report [17]. The existence of $Cu_{2-x}Se$ possibly helps to enhance the electrical properties, so all of our samples' electrical conductivity are higher. And we consider the ratio of three phases that are all generated by combustion process is the same. The increased densities also help to achieve higher electrical conductivity. The results of Seebeck coefficient in Figure 4b indicates the p-type behavior. The Seebeck coefficient is negatively correlated with electrical conductivity. The dip in the Seebeck coefficients at ~373 K is possibly caused by the disordered Cu atoms. Once heated to the temperature of 373 K, they start to move off from the original sites, which lead to the disorder situation gradually [23].

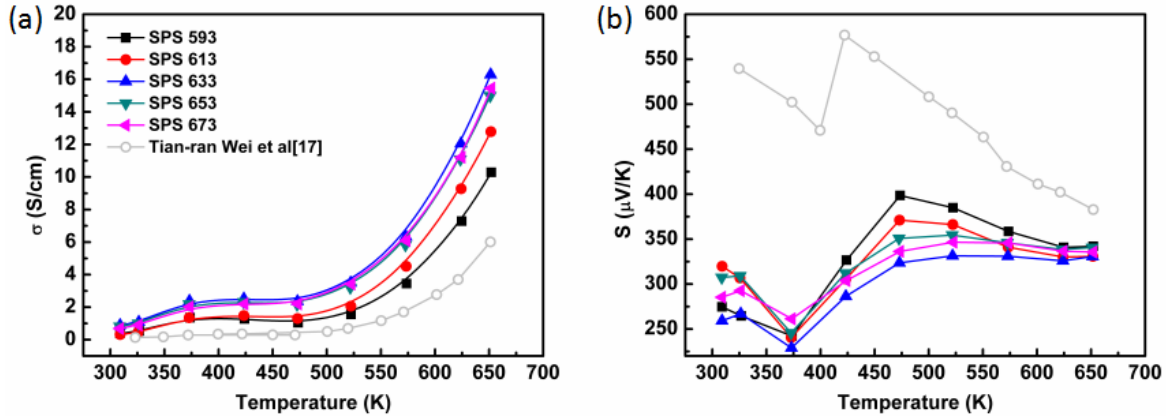


**Figure 4.** Temperature dependence of thermoelectric properties for all the samples with different SPS temperature and reference [17]: (**a**) electrical conductivity; and (**b**) the Seebeck coefficient.

$C_p$ is shown in Figure 5a. A peak appears at about 450 K which is because of the order–disorder transition of Cu atoms [14,23]. This transition was observed by a previous report [14] by high-temperature XRD. Their charge flipping analysis indicates that the disordered Cu atoms appeared above the transition temperature. The behavior of a phase transition combined with ordering of Cu atoms is similar to what was reported in the S and Bi-S analogs [24,25]. The ultralow thermal conductivity is shown in Figure 5b. κ decreases to about 0.30 $W \cdot m^{-1} \cdot K^{-1}$, which is probably associated with stronger anharmonicity and larger lattice resistance [12]. The disordered Cu atoms that are weakly

bonded to the lattice can easily vibrate along the c axis and have a great influence on phonon-phonon anharmonic processes which may partly block the heat transport [26].

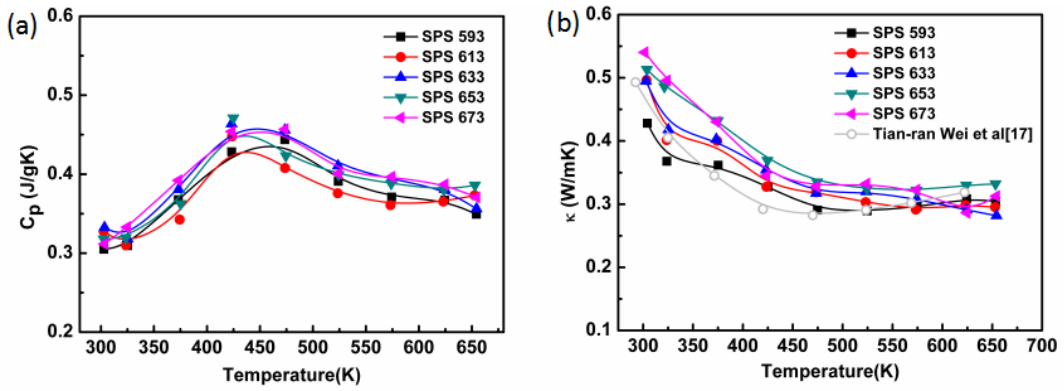


**Figure 5.** (**a**) $C_P$ and (**b**) κ of samples as functions of temperature with reported values by Wei et al. [17].

The calculated power factor (PF) reaches 1.8 $\mu W \cdot m^{-1} \cdot K^{-2}$ at 653 K as indicated in Figure 6a. The low electrical conductivity in the room temperature causes the low PF of $Cu_3SbSe_3$. Bases on the electrical and thermal transport data, and the dimensionless figure of merit ($ZT$) are shown in Figure 6b. The $ZT$ measurement uncertainty is about 15%. As mentioned above, the electrical conductivity was improved significantly but the thermal conductivity was almost unchanged. Therefore, the $ZT$ reflects an increasing trend with temperature, and the highest value of 0.42 at 653 K can be reached in the sample SPS 633, which is about 60% higher than in previous work [17] and the highest of all the $Cu_3SbSe_3$-based TE materials.

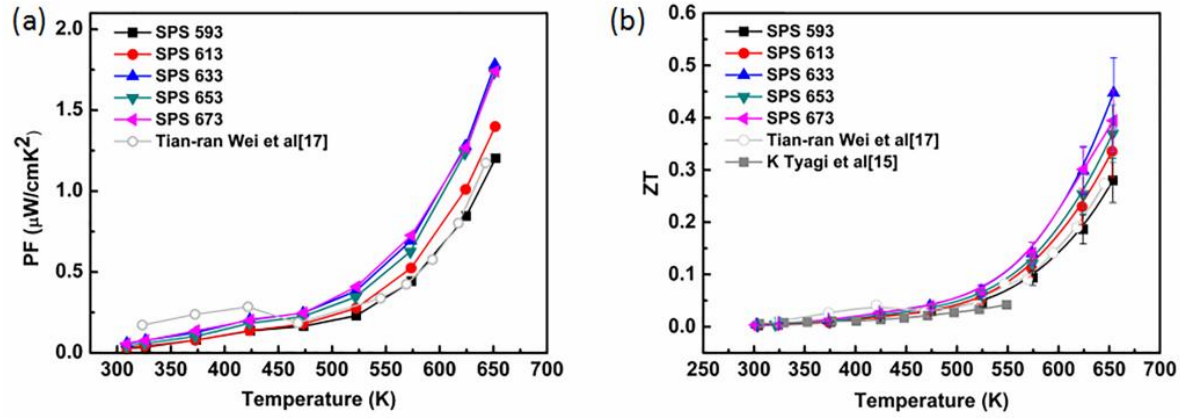


**Figure 6.** (**a**) Power factor and (**b**) $ZT$ as functions of temperature of the samples with different SPS temperature.

## 4. Conclusions

In summary, we used the SHS-SPS method to fabricate the $Cu_3SbSe_3$-based composites with $CuSeSb_2$ and $Cu_{2-x}Se$ as secondary phases. The ignition temperature of SHS approaches the lowest melting point (Se) of the compound. The existence of $Cu_{2-x}Se$ and the increased densities which were changed with SPS temperature enhanced the electrical conductivity, while the thermal conductivity changed slightly at high temperature. Finally, a maximum $ZT$ of 0.42 of the sample SPS 633 was obtained at 653 K due to the enhancement of electrical conductivity and low thermal conductivity, which is desirable for application in the mid-temperature range.

**Acknowledgments:** This work was supported by the Ministry of Science & Technology of China through a 973-Project, under Grant No. 2013CB632506, National Nature Science Foundation of China under Grant No. 51202232 and 11234012, the National Key Research Programme of China, under Grant No. 2016YFA0201003 and Specialized Research Fund for the Doctoral Program of Higher Education, under Grant No. 20120002110006.

**Author Contributions:** Rui Liu performed the experiments and wrote the paper. Guangkun Ren, Cewen Nan and Yuanhua Lin revised the manuscript. Xing Tan assisted in experiments.

**Conflicts of Interest:** The authors declare no conflict of interest.

## References

1. Snyder, G.J.; Toberer, E.S. Complex thermoelectric materials. *Nat. Mater.* **2008**, *7*, 105–114. [CrossRef] [PubMed]
2. Bell, L.E. Cooling, heating, generating power, and recovering waste heat with thermoelectric systems. *Science* **2008**, *321*, 1457–1461. [CrossRef] [PubMed]
3. Zhao, L.D.; Dravid, V.P.; Kanatzidis, M.G. The panoscopic approach to high performance thermoelectrics. *Energy Environ. Sci.* **2014**, *7*, 251–268. [CrossRef]
4. Wan, C.; Wang, Y.; Wang, N.; Norimatsu, W.; Kusunoki, M.; Koumoto, K. Development of novel thermoelectric materials by reduction of lattice thermal conductivity. *Sci. Technol. Adv. Mater.* **2010**, *11*. [CrossRef]
5. Zhao, L.D.; He, J.; Berardan, D.; Lin, Y.; Li, J.; Nan, C.; Dragoe, N. BiCuSeO oxyselenides: New promising thermoelectric materials. *Energy Environ. Sci.* **2014**, *7*, 2900–2924. [CrossRef]
6. Liu, H.L.; Shi, X.; Xu, F.F.; Zhang, L.L.; Zhang, W.Q.; Chen, L.D.; Li, Q.; Uher, C.; Day, T.; Snyder, G.J. Copper ion in liquid-like thermoelectrics. *Nat. Mater.* **2012**, *11*, 422–425. [CrossRef] [PubMed]
7. Zhao, L.D.; Lo, S.H.; Zhang, Y.; Sun, H.; Tan, G.; Uher, C.; Wolverton, C.; Dravid, V.P.; Kanatzidis, M.G. Ultralow thermal conductivity and high thermoelectric figure of merit in SnSe crystals. *Nature* **2014**, *508*, 373–377. [CrossRef] [PubMed]
8. Chen, L.D.; Wang, H.; Chen, Y.Y.; Day, T.; Snyder, G.J. Thermoelectric properties of p-type polycrystalline SnSe doped with Ag. *J. Mater. Chem. A* **2014**, *2*, 11171–11176. [CrossRef]
9. Wei, T.R.; Wang, H.; Gibbs, Z.M.; Wu, C.F.; Snyder, G.J.; Li, J.F. Thermoelectric properties of Sn-doped p-type $Cu_3SbSe_4$: A compound with large effective mass and small band gap. *J. Mater. Chem. A* **2014**, *2*, 13527–13533. [CrossRef]
10. Zhang, Y.; Ozolin, V.; Morelli, D.; Wolverton, C. Prediction of new stable compounds and promising thermoelectrics in the Cu-Sb-Se System. *Chem. Mater.* **2014**, *26*, 3427–3435. [CrossRef]
11. Lu, X.; Morelli, D.T.; Xia, Y.; Zhou, F.; Ozolins, V.; Chi, H.; Zhou, X.; Uher, C. High performance thermoelectricity in earth-Abundant compounds based on natural mineral tetrahedrites. *Adv. Energy Mater.* **2013**, *3*, 342–348. [CrossRef]
12. Zhang, Y.; Skoug, E.; Cain, J.; Ozolin, V.; Morelli, D.T.; Wolverton, C. First-principles description of anomalously low lattice thermal conductivity in thermoelectric Cu-Sb-Se ternary semiconductors. *Phys. Rev. B* **2012**, *85*. [CrossRef]
13. Skoug, E.J.; Morelli, D.T. Role of lone-pair electrons in producing minimum thermal conductivity in nitrogen-group chalcogenide compounds. *Phys. Rev. Lett.* **2011**, *107*. [CrossRef] [PubMed]
14. Kirkham, M.; Majsztrik, P.; Skoug, E.; Morelli, D.; Wang, H.; Porter, W.D.; Payzant, E.A.; Lara-Curzio, E. High-temperature order/disorder transition in the thermoelectric $Cu_3SbSe_3$. *J. Mater. Res.* **2011**, *26*, 2001–2005. [CrossRef]
15. Tyagi, K.; Gahtori, B.; Bathula, S.; Toutam, V.; Sharma, S.; Singh, N.K.; Dhar, A. Thermoelectric and mechanical properties of spark plasma sintered $Cu_3SbSe_3$ and $Cu_3SbSe_4$: Promising thermoelectric materials. *Appl. Phys. Lett.* **2014**, *105*. [CrossRef]
16. Majsztrik, P.W.; Kirkham, M.; Garcia-Negron, V.; Lara-Curzio, E.; Skoug, E.T.; Morelli, D.T. Effect of thermal processing on the microstructure and composition of Cu-Sb-Se compounds. *J. Mater. Sci.* **2013**, *48*, 2188–2198. [CrossRef]
17. Wei, T.R.; Wu, C.F.; Sun, W.; Pan, Y.; Li, J.F. Is $Cu_3SbSe_3$ a promising thermoelectric material? *RSC Adv.* **2015**, *5*, 42848–42854. [CrossRef]

18. Su, X.; Fu, F.; Yan, Y.; Zheng, G.; Liang, T.; Zhang, Q.; Cheng, X.; Yang, D.; Chi, H.; Tang, X. Self-propagating high-temperature synthesis for compound thermoelectrics and new criterion for combustion processing. *Nat. Commun.* **2014**, *5*. [CrossRef] [PubMed]
19. Rouessac, F.; Ayral, R.M. Combustion synthesis: A new approach for preparation of thermoelectric zinc antimonide compounds. *J. Alloys Compd.* **2012**, *530*, 56–62. [CrossRef]
20. Selig, J.; Lin, S.; Lin, H.T.; Johnson, D. Combustion synthesis of doped thermoelectric oxides. *J. Aust. Ceram. Soc.* **2012**, *48*, 194–197.
21. Yi, H.; Moore, J. Self-propagating high-temperature (combustion) synthesis (SHS) of powder-compacted materials. *J. Mater. Sci.* **1990**, *25*, 1159–1168. [CrossRef]
22. Munir, Z.A.; Munir, J.B. *Combustion and Plasma Synthesis of High-Temperature Materials*; Wiley-VCH: Hoboken, NJ, USA, 1990.
23. Samanta, K.; Gupta, N.; Kaur, H.; Sharma, H.; Pandey, S.D.; Singh, J.; Senguttuvan, D.T.; Sharma, N.D.; Bandyopadhyay, A.K. Order–disorder transition and Fano-interference in thermoelectric $Cu_3SbSe_3$ nanoparticles. *Mater. Chem. Phys.* **2015**, *151*, 99–104. [CrossRef]
24. Pfitzner, A. Disorder of $Cu^+$ in $Cu_3SbS_3$: Structural investigation of the high- and low-temperature modification. *Cryst. Mater.* **1998**, *213*, 228–236. [CrossRef]
25. Makovicky, E. Polymorphism in $Cu_3SbS_3$ and $Cu_3BiS_3$—The ordering schemes for copper atoms and electron-microscope observations. *Neues Jahrbuch für Mineralogie - Abhandlungen* **1994**, *168*, 185–212.
26. Qiu, W.; Wu, L.; Ke, X.; Yang, J.; Zhang, W. Diverse lattice dynamics in ternary Cu-Sb-Se compounds. *Sci. Rep.* **2015**, *5*. [CrossRef] [PubMed]